Hindawi
International Journal of Photoenergy
Volume 2022, Article ID 7225179, 15 pages
https://doi.org/10.1155/2022/7225179

Research Article

Feature-Reduced Stability Analysis of Islanded Photovoltaic Microgrid Inverters

A. Om Prakash [1] **and R. Narmatha Banu** [2]

[1]*Department of EEE, Government Polytechnic College, Usilampatti, Madurai, India*
[2]*Department of EEE, Velammal College of Engineering and Technology, Madurai, India*

Correspondence should be addressed to A. Om Prakash; aop@vcet.ac.in

Received 27 February 2022; Revised 4 October 2022; Accepted 20 October 2022; Published 21 November 2022

Academic Editor: Gianluca Coccia

A smart grid environment is prone to data explosion while controlling a microgrid system. Islanded Microgrid's stability analysis involves a large number of system state variables thus consuming more computational memory due to parallel connected inverter dynamics. Parallel inverters generate reference voltage and frequency using droop controllers, unlike grid-connected inverters where the primary grid provides the reference voltage and frequency. This paper develops feature-reduced stability analysis of the parallel inverters thus reducing the computational memory of its stability analysis. Principal component analysis being a feature extraction technique is applied to reduce the number of variables determining stability. MATLAB is used to develop the average model of a parallel inverter with an LCL filter and a three-phase AC load. Evaluation of the stability analysis using the state variable analysis with the virtual resistance method is simulated. Simulation validates stability analysis of the model with reduced state variables. An average model developed using MATLAB and PCA carried out using Python clearly indicated the validation of the dimensionality reduction in the stability analysis. The reduced number of variables is validated for a stable range of the parallel inverter droop controller. Both cases validated the dimensionality reduction in the stability analysis of parallel inverters.

1. Introduction

Renewable energy-based power generators connected to the distribution system are called distributed energy resources (DERs). DERs from different renewable sources form a microgrid. The microgrid, with its dynamic nature, needs stability analysis to understand the stability limits during disturbances in the system. Stability analysis uses state variables that impact the system's stability. Adopting smart technologies in the microgrid environment reckons exponential use of data since it involves localized power generation, independent power control, and dependency primarily on renewable sources. State variables are collected as data using smart devices. Microgrid facilitates the supply of remote end loads by grid-connected or islanded mode of operation. Grid-connected mode of operation uses decoupled controllers (direct axis/quadrature axis controller (DQ) and instantaneous real/reactive power (PQ)) for synchronizing renewable energy to the main grid. Synchronization is maintaining the same voltage level and phase angle among parallel inverters using control techniques (Rodríguez-Cabero [1]). The higher penetration level of renewable energy in a power system promises microgrid's islanded mode of operation possible [2, 3]. Islanded mode of operation is a complex model involving many state variables for its stability analysis. Microgrid environments adopt soft computing techniques in the energy management system Leonori et al. [4] and load frequency controller (LFC) Gheisarnejad and Khooban [5]. Due to the absence of grid power in islanded mode, droop controllers employ autonomous operation to manage synchronism Firdaus and Mishra [6] and reactive power sharing problems (Zandi et al. [7]). Inverters supplied by renewable energy and connected to a common load are called parallel inverters. The islanded mode of Microgrid's operation uses a parallel inverter structure that synchronizes with a droop controller. Rasheduzzaman et al. [8] applied

stability analysis of parallel inverters using Eigen analysis on the average model.

State space variables from the average model are obtained for Eigen analysis. Stability analysis of the autonomous microgrid that combines diesel and a renewable energy source is investigated. The droop control strategy is chosen among the different controls by comparing the controller performance with Veerashekar et al. [9]. Intentional, active power reduction from renewable sources caused the loss in the diesel generator during the fault condition. At the same time, the postfault recovery demanded complete reactive power from renewable energy (Veerashekar et al. [9]). Dag M and M T [10] discuss the stability of the low voltage (LV) inverter-based microgrid. Inverter-fed distributed system supplied by two inverters is applied to the harmonic instability analysis (Wang et al. [11]). Multiple parallel inverters connected deteriorate the impedance-based method of analysis. Researchers used aggregation of inverters to implement the parallel inverter stability analysis accurately. The small signal analysis of each component in the droop-controlled parallel inverter-based distribution system is applied (Rodríguez-Cabero and [1]). The parallel inverter distribution system's critical network settings and control parameters are estimated. An impedance-based stability criterion is used to analyze the stability of multiple parallel inverters connected to the grid (Alenius et al. [12]).

Offshore long cable parallel inverters are inducted for impedance-based stability analysis Zhang et al. [13]. Nonnegligible long cables and three different inverters are adopted for stability analysis. Unlike previous stability analyses, dissimilar inverters and characteristics of the cables are considered by Zhang et al. [13].

Discussions on impedance-based and eigenvalue-based small signal stability analysis implementation are limited to a few states as they require analysis of source load subsystems (Amin and Molinas [14]). Literature surveys discusses an advanced impedance-based controller for parallel inverters controlled by both PQ-based impedance and droop controller-based methods. Double-closed-loop controlled parallel inverters use the impedance method for stability analysis. Droop controllers are a more frequently used synchronization technique in the above publications.

This paper exploits soft computing methods for feature-reduced stability analysis of parallel inverters. The proposed approach applies principal component analysis (PCA) to a set of state variables to reduce the number of state variables used for eigenvalue-based stability analysis. State variables chosen from the parallel inverter's average model that affect the actual steady state analysis of the parallel inverters are obtained from the PCA. Eigen analysis of state variables on the average model developed from MATLAB is observed. PCA extracted using Python defines the critical variables that affect the stability of the average model. Droop control of parallel inverters is detailed in Section 2. Section 3 and Section 4 elaborate on the results and discussion, followed by the conclusion and references.

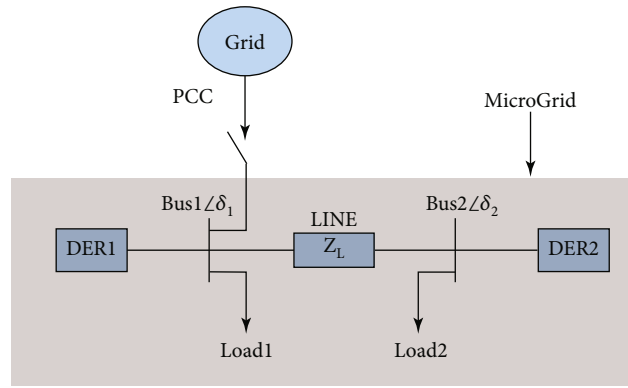

Figure 1: Islanded Microgrid Parallel Inverters.

2. Droop-Controlled Inverters

Traditional grid-connected (PV) comprises an energy source and an inverter. The main grid's voltage and phase angle reference synchronize the inverter with the grid. In weak grid conditions (mode), the inverters connected in parallel need self-synchronization. Two parallel connections are shown in Figure 1.

Exploiting the stochastic nature of the inverters, one is used as a reference inverter and the other as a slave inverter. DER1 and DER2 are photovoltaic power generators connected in parallel in the islanded mode. ZL is the impedance of the three-phase AC line between the photovoltaic generators. The droop controller of the parallel inverters adopted the droop characteristics. The voltage and frequency of the VSI changed with reactive and real power, respectively. The slope from $(P-\omega)$ and $(Q-V)$ curves is obtained to develop the droop controller for synchronization. For high-frequency noise attenuation from the inverter, the LCL filter is utilized.

Droop controller block diagram is defined in Figure 2. The droop controller maps the voltage and phase angle from the real and reactive power calculated from the droop characteristics curve. Oscillation in real and reactive power is filtered using the low pass filter to get a steady waveform. Synchronous reference frame (SRF) reference voltage and phase angle from the droop controller regulated the synchronization between the inverters. Voltage and phase angle generated from the phase-locked loop (PLL) at the load is compared with the droop characteristic curve. One of the two parallel inverters acted as the master and the other as the slave. The voltage and phase angle of the master inverter is followed by the slave inverter. It is assumed that the photovoltaic source is providing a constant DC voltage as the input to the parallel inverters.

2.1. Parallel Inverter State Space Modeling. The inverter is designed to operate based on droop characteristics which originate from the principles of power balance in synchronous generators. The droop characteristics allow power sharing between distributed grids. For modeling the dynamic behavior of the inverter, we chose state space modelling. The different components of the inverters are also modelled in the state space.

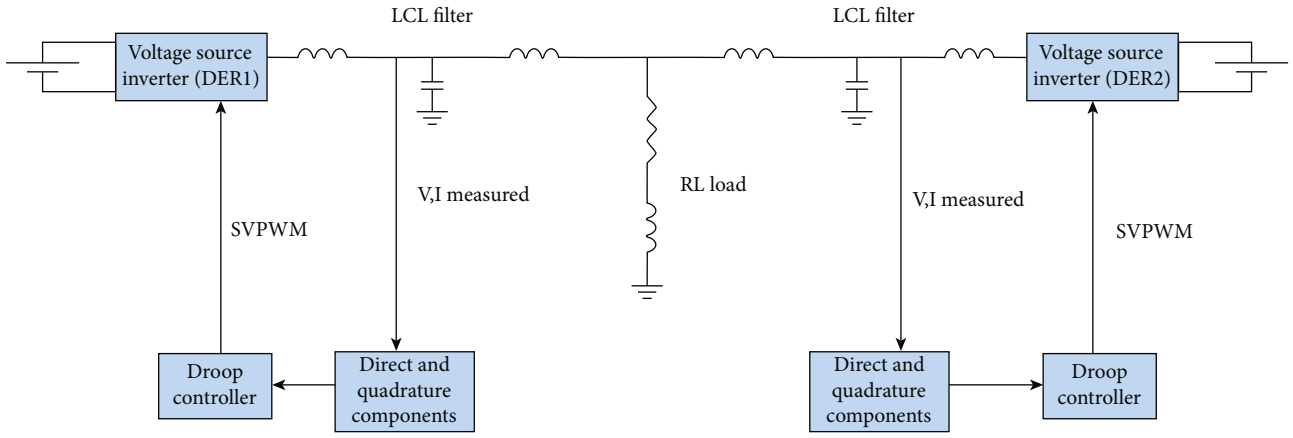

Figure 2: Droop controller overall block diagram.

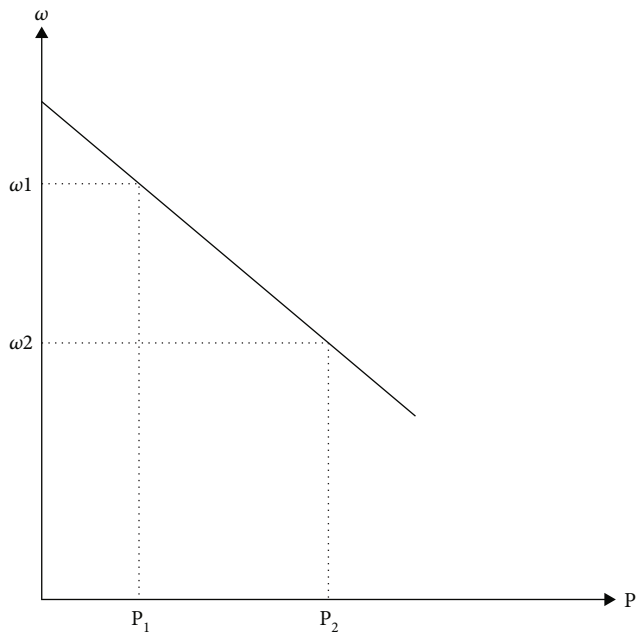

Figure 3: Droop characteristics $P-\omega$ curve.

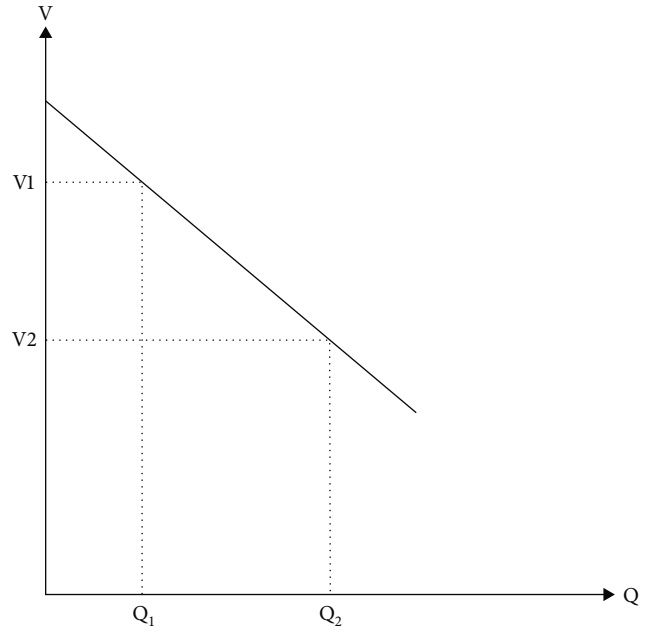

Figure 4: Droop characteristics $Q-V$ curve.

$$p = \frac{3}{2}\left(v_{od}i_{od} + v_{oq}i_{oq}\right), \tag{1}$$

$$q = \frac{3}{2}\left(v_{oq}i_{od} - v_{od}i_{oq}\right). \tag{2}$$

Here, v_{od}, i_{od}, v_{oq}, and i_{oq} are direct axis voltage, current, quadrature axis voltage, and current before the capacitor in LCL filter.

2.2. Inverter Model. Instantaneous power at the inverter output is given below. Real power is defined by Equation (1), while Equation (2) defines the reactive power. Both real and reactive power are calculated from the synchronous reference frame components of the voltage (v_{od}, v_{oq}) and current (i_{od}, i_{oq}) measured,

$$P = \frac{\omega_c}{s+\omega_c}p = -P\omega_c + 1.5\omega_c\left(v_{od}i_{od} + v_{oq}i_{oq}\right), \tag{3}$$

$$Q = \frac{\omega_c}{s+\omega_c}q = -Q\omega_c + 1.5\omega_c\left(v_{oq}i_{od} - v_{od}i_{oq}\right), \tag{4}$$

where ω_c is the corner frequency.

2.3. Droop Characteristics. Generally, the internal reference voltage and angle are obtained from the grid. During weak grid conditions, the inverter generates the reference from droop characteristics which mimic the operation of a synchronous motor. Droop characteristic $P-\omega$ and $Q-V$ curves are shown in Figures 3 and 4, respectively. In addition, during autonomous operation, when the inverter is operating in the islanded mode, self-synchronizing is achieved by using the slopes of $P-\omega$ and $Q-V$ curves (which are set before hand) (Rasheduzzaman et al. [8]).

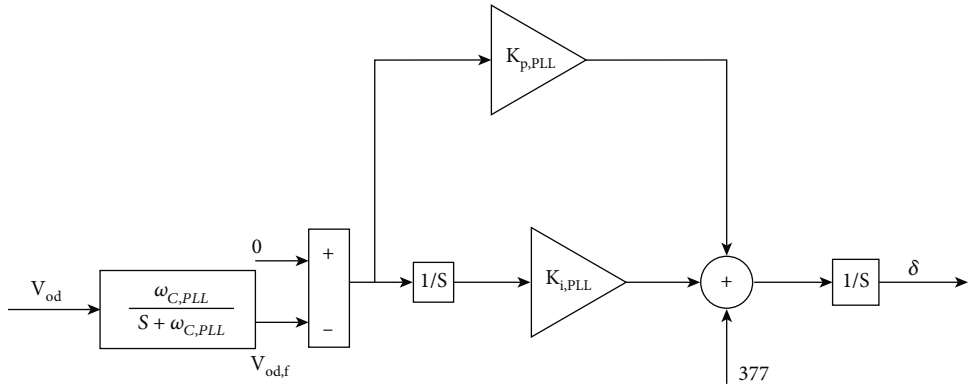

Figure 5: PLL module.

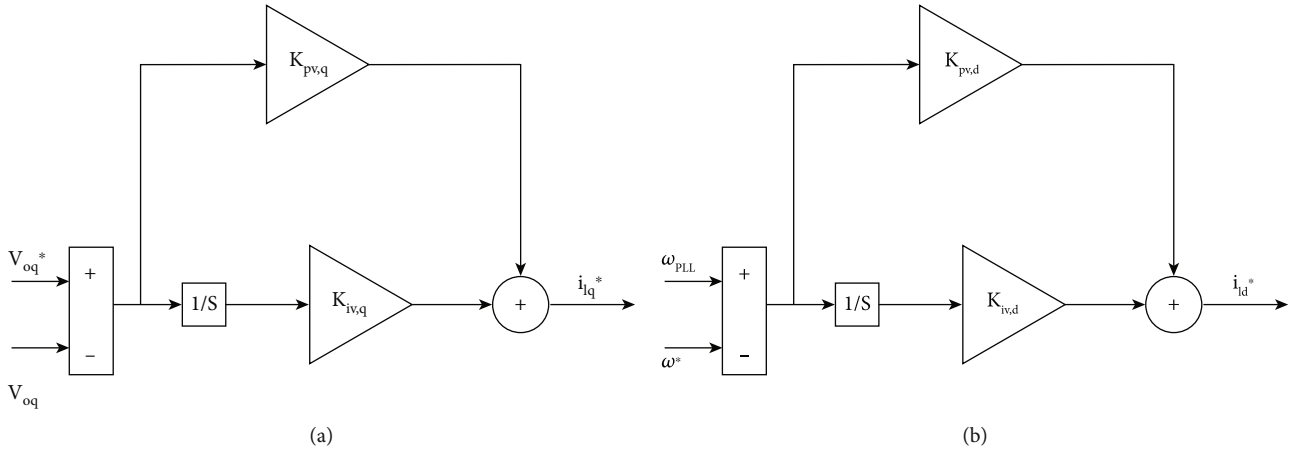

Figure 6: Voltage controller (a), quadrature axis current reference, and (b) direct axis current reference.

Slopes of $P-\omega$ and $Q-V$ are m and n, respectively, given in

$$m = \frac{\omega_1 - \omega_2}{P_2 - P_1}, \tag{5}$$

$$n = \frac{v_1 - v_2}{Q_2 - Q_1}. \tag{6}$$

Instantaneous real and reactive power is used to obtain the voltage and angular frequency values using Equations (5) and (6). The reference angular frequency and reference voltage are obtained from the equations that are shown below in Equations (7) and (8). These equations provide the reference voltage and angular rad/sec.

$$\omega^* = \omega_n - mP, \tag{7}$$

$$v_{oq}^* = v_{oq,n} - nQ. \tag{8}$$

where ω_1, ω_2 are different angular frequency instants from the droop curve from Figure 3. While P_1, P_2 are real power amplitude instance at the inverter output when sinusoidal output with 60 Hz is delivered. Instantaneous angular frequency ω_n when applied for synchronization in the parallel inverters, $v_{oq,n}$ is the instantaneous quadrature axis voltage component. Reference angular frequency ω^* and reference quadrature axis voltage component v_{oq}^* for synchronization is calculated using the Equations (7) and (8).

2.4. Phase-Locked Loop (PLL). Actual voltage and angular rad/sec are obtained from PLL as shown in Figure 5. It is a PI-based PLL controller that generates input to the voltage and current controllers. The input to be compared is first filtered by a low pass filter of corner frequency $\omega_{c,pll}$. Since synchronization frequency must be constant, the ω_{PLL} is compared with 377 (rad/sec for 60 Hz) to generate instantaneous angle (δ) from the phase-locked loop.

The direct axis voltage is locked to zero in the PLL. During the autonomous inverter's operation, the PLL is responsible for synchronizing the frequency with that of the main inverter.

2.5. Voltage Controller. The voltage controller is comprised of two PI controllers. The voltage and phase angle are compared for both actual and droop characteristics to obtain the droop control. The PI controllers for the reference current generation obtained from the controller are shown in Figure 6.

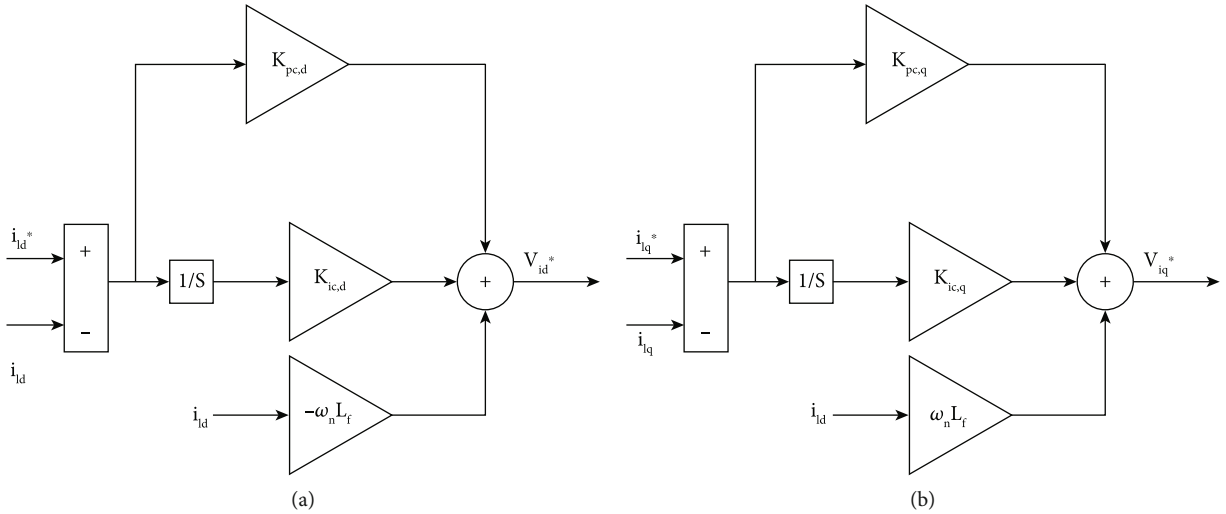

Figure 7: Current controller (a) quadrature axis voltage reference, (b) direct axis voltage reference.

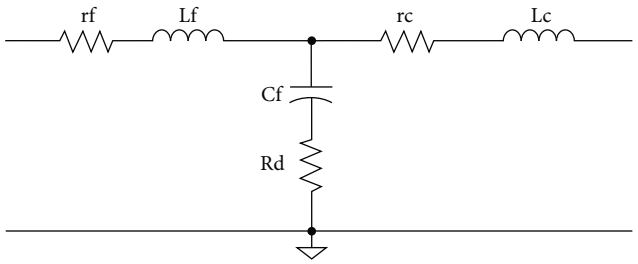

Figure 8: LCL filter circuit.

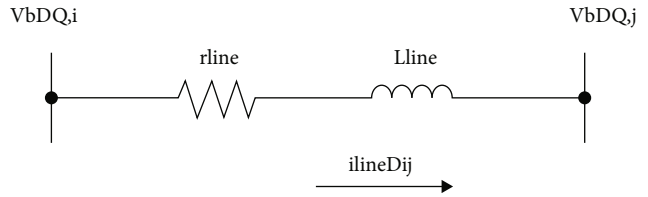

Figure 10: Distribution line.

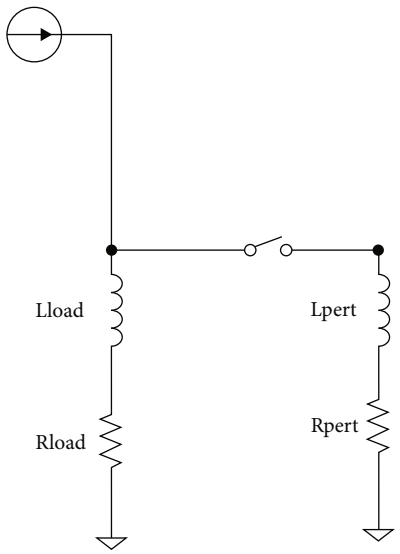

Figure 9: Load configuration.

The voltage controller uses a PI controller to generate the reference current. The state equation for the voltage controller is given as,

$$\Phi_d' = \omega_{PLL} - \omega^* \; ; \; i_{ld}^* = k_{iv,d}\Phi_d + k_{pv,d}\Phi_d', \tag{9}$$

$$\Phi_q' = v_{oq}^* - v_{oq} \; ; \; i_{lq}^* = k_{iv,q}\Phi_q + k_{pv,q}\Phi_q', \tag{10}$$

where Φ_d' *is* the angular rad/sec difference with the reference, Φ_q' is the voltage difference with the reference, obtained from the droop characteristics.

The direct axis reference current i_{ld}^* after the filter capacitor and quadrature axis reference current i_{lq}^* after the filter capacitor (LCL) are calculated using the Equations (9) and (10). Integral and proportional gain $k_{iv,d}, k_{pv,d}$ to generate direct axis reference current and $k_{iv,q}, k_{pv,q}$ for quadrature axis reference current is used as in Equations (9) and (10). This is depicted in Figure 6.

2.6. Current Controller. The voltage controller's output is fed to the current controller. PI controller compares the current from the droop controller and the actual is measured. The input to the current reference is fed into the voltage controller. The comparator compared the reference and the measured currents from the output of the LCL filter. The output of the current controller is the reference voltage v i^*_{dq}. This comparison controlling the inverter using the space sector PWM (SVPWM) is generated from the current controller as shown in Figure 7.

The state equation is shown below in Equations (11) and (12) to generate direct axis voltage reference v_{id}^* and

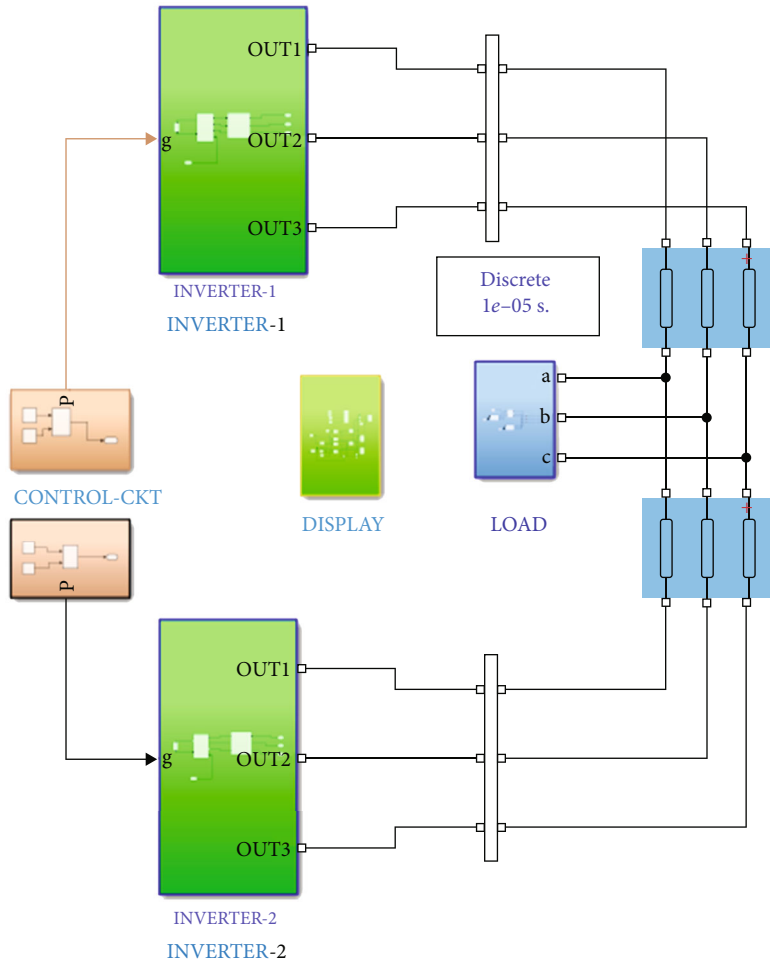

Figure 11: Overall simulation diagram-feature reduced stability analysis.

quadrature axis voltage reference v_{iq}^{*}.

$$v_{id}^{*} = -\omega_n L_f i_{lq} + k_{ic,d}\sum(i_{\mathrm{ld}}^{*} - i_{ld}) + k_{pc,d}\sum(i_{ld}^{*} - i_{ld}), \quad (11)$$

$$v_{iq}^{*} = -\omega_n L_f i_{ld} + k_{ic,q}\sum\left(i_{lq}^{*} - i_{lq}\right) + k_{pc,q}\sum\left(i_{lq}^{*} - i_{lq}\right), \quad (12)$$

where $k_{pc,d}$, $k_{ic,d}$ are proportional and integral gain of PI controller to generate direct axis voltage reference, while $k_{pc,q}$, $k_{ic,q}$ are proportional and integral gain to generate quadrature voltage gain. Input given to the PI controller is the difference of actual (without *) and reference direct (i_{ld}^{*}, i_{ld}) and quadrature (i_{lq}^{*}, i_{lq}) current.

2.7. LCL Filter. The LCL filter for the inverter is designed without considering the losses in the IGBTs and diodes. Command voltage generated from the current controller is sent to the LCL filter. The LCL filter with its inherent resistance values is depicted in Figure 8.

The two inductors, L_f and L_c have parasitic resistances r_f and rc, respectively. The filter capacitor C_f along with the damping resistor R_d are connected as part of the LCL filter. The state equation governing the filter characteristics of the LCL filter is shown below.

$$i_{ld}'' = \frac{1}{L_f}\left(-r_f i_{ld} + v_{id} + v_{od}\right) + \omega_{PLL} i_{lq}, \quad (13)$$

$$i_{lq}'' = \frac{1}{L_f}\left(-r_f i_{lq} + v_{iq} + v_{oq}\right) + \omega_{PLL} i_{ld}. \quad (14)$$

Equation (13) defines the direct axis current (i_{ld}'') and Equation (14) defines quadrature axis current i_{lq}'' from the inductor to the capacitor in the LCL filter.

$$i_{od}'' = \frac{1}{L_c}\left(-r_c i_{oq} + v_{od} - v_{bd}\right) - \omega_{PLL} i_{oq}, \quad (15)$$

$$i_{oq}'' = \frac{1}{L_c}\left(-\mathrm{r}_c i_{od} + v_{oq} - v_{bq}\right) - \omega_{PLL} i_{od}. \quad (16)$$

Equation (15) defines the direct axis current (i_{ld}'') and Equation (16) defines quadrature axis current (i_{lq}'') from

Table 1: Parameter value.

Parameter	Value
rc	0.09 Ω
L_f	4.20 mH
r_f	0.50 Ω
Lc	0.50 mH
R_d	2.2025
C_f	15 uF
ωc	50.26 rad/s
$\omega_{c,pll}$	7853.98 rad/s
m	1/1000 rad/Ws
n	1/1000 V/var
rn	1000
R_{load}	25 Ω
L_{load}	15 mH
Rpert	25 Ω
Lpert	7.50 mH
r_{line}	0.15 Ω
L_{line}	0.40 mH
Voq, n	85 V
ωn	377 rad/s
ω_{pll}	377 rad/s

the capacitor to load side inductor in the LCL filter.

$$v'_{od} = \frac{1}{C_f}(i_{ld} - i_{od}) + \omega_{PLL} v_{oq} + R_d(i_{ld} - i_{od}), \tag{17}$$

$$v'_{oq} = \frac{1}{C_f}\left(i_{lq} - i_{oq}\right) + \omega_{PLL} v_{od} + R_d\left(i_{lq} - i_{oq}\right). \tag{18}$$

Equations (17) and (18) define the load side direct and quadrature axis voltage v'_{od} and v'_{oq}, respectively, in LCL filter.

2.8. Load Perturbation. An RL load is introduced during the inverter operation to study the dynamic behavior. The steady state output frequency and voltage are evaluated. Figure 9 depicts the load configuration of the load perturbation added as the load to the inverter. R_{load} and L_{load} are taken as load resistance and inductance, and the perturbation resistance and inductance are defined as R_{pert} and L_{pert} . The perturbation elements are used for the stability analysis of the parallel inverters with load dynamics introduced using these elements.

The state equation describing the dynamic behavior is shown below in Equations (19) and (20). Load direct axis current ($i_{\text{load}D}$) and load quadrature axis current ($i_{\text{load}Q}$) are as given in Equations (19) and (20).

$$i_{\text{load}D} = \frac{1}{L_{\text{load}}}(-R_{\text{load}} i_{\text{load}D} + V_{bD}) + \omega_{pll} i_{\text{load}Q}, \tag{19}$$

$$i_{\text{load}Q} = \frac{1}{L_{\text{load}}}\left(-R_{\text{load}} i_{\text{load}Q} + V_{bQ}\right) - \omega_{pll} i_{\text{load}D}. \tag{20}$$

The introduction of capacitive load during load perturbation is a novel study carried out in this paper, which helped us evaluate the dynamic response of the inverter under autonomous operation.

2.9. Distribution Line. The distribution line represents the lumped resistance and inductor similar to that of the load. Since these wires are connected to other inverters in the distributed grid, the resistance and inductance play important roles in the response of the inverter during load perturbation. The state equation describing the distribution line is shown below in Equations (21) and (22). The line configuration for this parallel inverter setup is given in Figure 10. Subscript "i" is of DER1 and subscript "j" is of DER2. Distribution line is connected between these two DERs as given in Figure 10. Direct axis current ($i_{\text{line}Dij}$) and quadrature axis current ($i_{\text{line}Qij}$) between "i" to "j" DERs.

$$i_{\text{line}Dij} = \frac{1}{\bar{L}_{\text{line}}}\left(r_{\text{line}} i_{\text{line}D} + v_{bD,i} - v_{bD,j}\right) + \omega_{\text{pll}} i_{\text{line}Q}, \tag{21}$$

$$i_{\text{line}Qij} = \frac{1}{\bar{L}_{\text{line}}}\left(r_{\text{line}} i_{\text{line}Q} + v_{bQ,i} - v_{bQ,j}\right) + \omega_{\text{pll}} i_{\text{line}D}, \tag{22}$$

where r_{line} is line resistanc, $\bar{L}_{line}$ is the line inductance, between two DERs and $v_{bD,i} v_{bQ,i}$ direct and quadrature voltage at the line in the "i^{th}" DER. $v_{bQ,i}, v_{bQ,j}$ are direct and quadrature voltage at "j^{th}" DER.

The average model of this parallel inverter is used to obtain the state variables. These state variables are linearized to obtain stability analysis using Eigen analysis.

MATLAB average model is developed as given in the following section for the mathematical model defined in this section.

2.10. Simulation Setup. MATLAB-based simulation is setup and developed to obtain the average model of the mathematical description in previous section. The overall simulation diagram of the average model is as given in Figure 11. Two three inverters considered to be supplied from PV panels are assumed to supply constant DC voltage. Designated with name Inverter 1 and Inverter2, these two inverters are controlled using the droop characteristics to obtain synchronism between them. An LCL filter is used at the inverter output to filter the output to obtain sinusoidal output voltages. Line impedance and RL load are designed that can vary overtime. PI controller parameters are adjusted to obtain synchronism in the voltage waveform of both the inverters. Droop controller is designated as "Control Circuit" for both the inverters. The simulation is developed for 4 secs duration in both lower load (steady state) and higher load conditions (unsteady state). The results obtained are as given in the

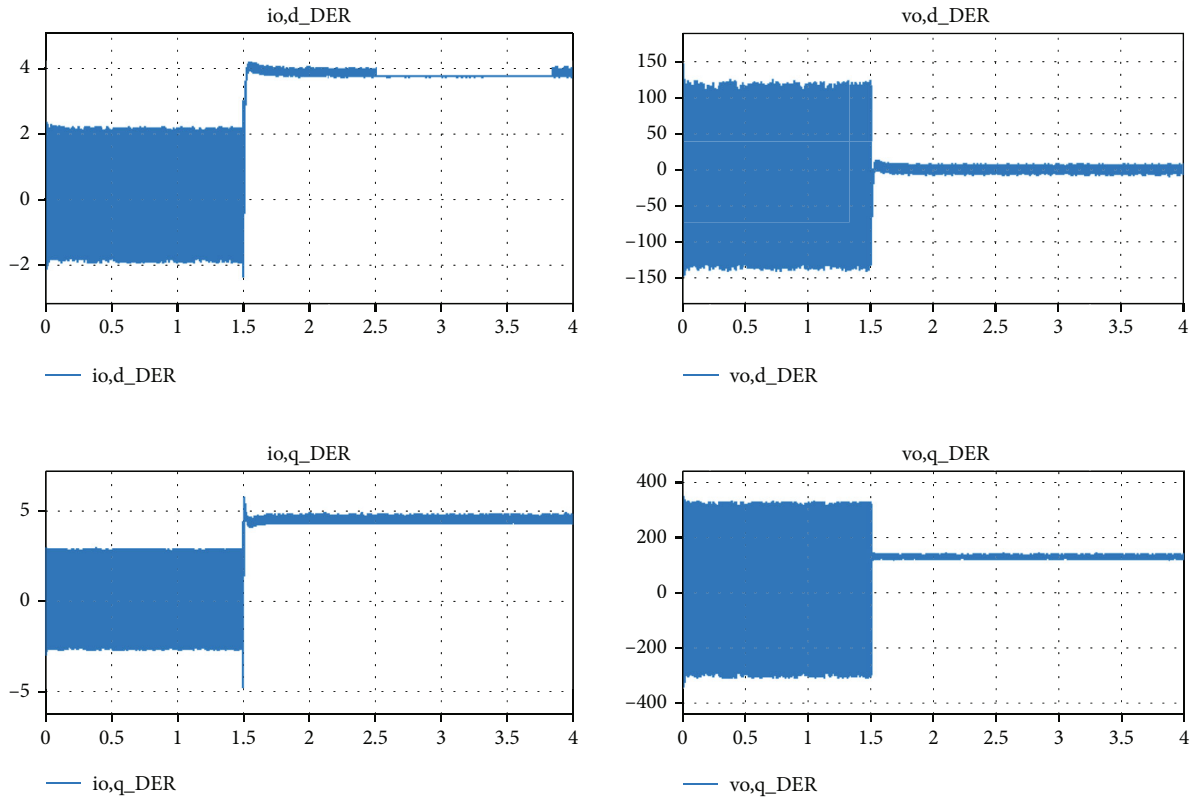

Figure 12: Photovoltaic Generators, Direct and Quadrature-voltage and current.

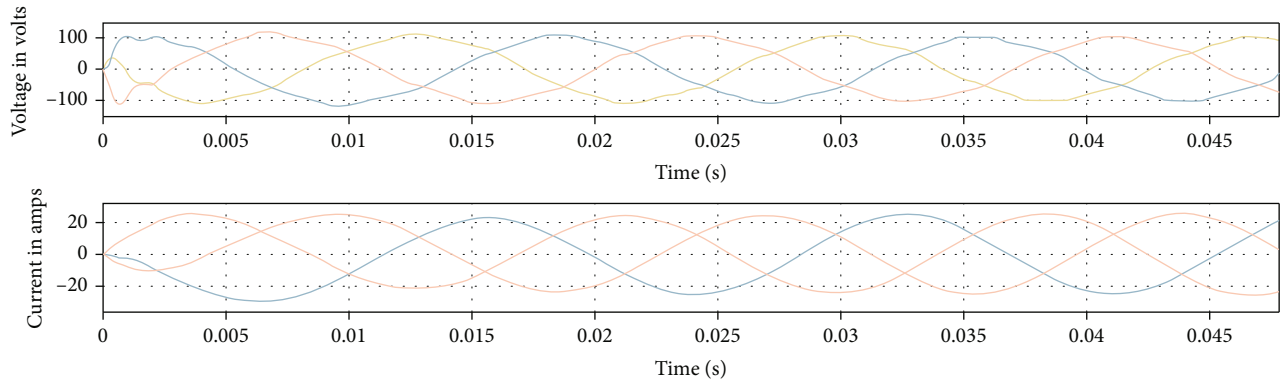

Figure 13: Voltage and current waveform of a photovoltaic generator.

following section. The parameters used for simulation are shown in Table 1.

The average model of the parallel inverter is developed using MATLAB Simulink using the parameters used in Table 1. MATLAB simulation developed as per Figure 11 is used for stability analysis and feature reduction analysis as given in the following section.

3. Results

Photovoltaic generator output is discussed in Figure 12. Both direct and quadrature components are obtained, while a load variation in the perturbation impedance at 1.5 secs is introduced. The mode changed from stable to unstable mode when the load impedance is changed drastically.

The voltage and current waveform obtained in the steady state operation are as shown in Figure 13. Waveforms of both parallel inverters are similar during steady state operation.

The radians and radians/secs during the steady operation of both inverters are shown in Figures 14 and 15, respectively. The angular radians/sec of 377 corresponding to 60 Hz is maintained in both inverters during the steady state operation.

The angular radians/sec for both the photovoltaic generators are shown in Figure 16. The variation between the

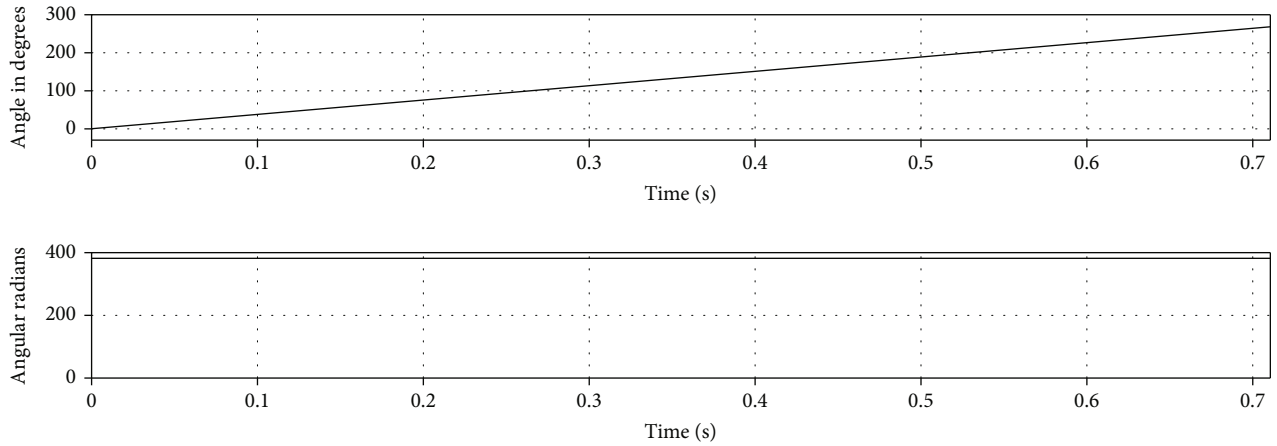

Figure 14: Angular radians and radians/sec for DER1.

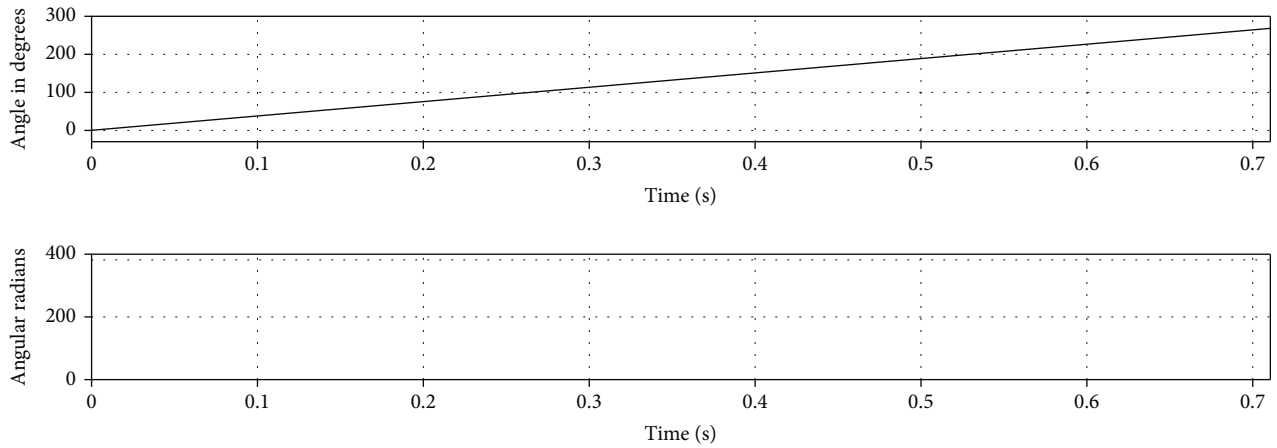

Figure 15: Angular radians and radians/sec for DER2.

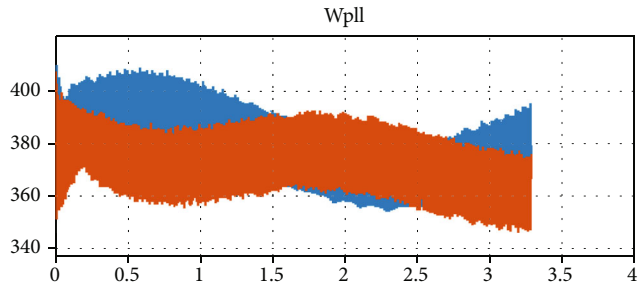

Figure 16: Angular rad/sec during stable region.

angular variations of both photovoltaic generators during the steady state region is found to be very close to each other.

Variation in the angular rad/sec is near the actual desired 377 corresponding to 60 Hz. Due to higher load, controller oscillations in the inverter are higher. Thus, the variation of angular rad/sec is more oscillatory. Due to the higher load variation in the slave photovoltaic generators, its angular rad/sec varied as shown in Figure 17.

Perturbation in the load is increased to the unstable region also to validate the dimensionality reduction for stability analysis. Real and reactive power variations in the unstable region are shown in Figure 18. A negative reactive power is observed in the slave photovoltaic generators.

A total of 36 states completely describe the two full inverters. These states are defined in the following array. x_{inv1},x_{inv2}, and x_{load} are state variables of DER1, DER2, and load, respectively. Linearization of these variables is the collection of these state variables, equilibrium values, or the steady state values, given as

$$x_{inv1} = \left(\delta_1 P_1 Q_1 \Phi_{d1} \Phi_{q1} \gamma_{d1} \gamma_{q1} i_{ld1} i_{lq1} v_{od1} v_{oq1} i_{od1} i_{oq1} \Phi_{PLL1} v_{od1,f}\right), \tag{23}$$

$$x_{inv2} = \left(\delta_2 P_2 Q_2 \Phi_{d2} \Phi_{q2} \gamma_{d2} \gamma_{q2} i_{ld2} i_{lq2} v_{od2} v_{oq2} i_{od2} i_{oq2} \Phi_{PLL2} v_{od2,f}\right), \tag{24}$$

$$x_{\text{load}} = \left[i_{\text{load}D1}\ i_{\text{load}Q1}\ i_{\text{load}D2} i_{\text{load}Q2}\right], \tag{25}$$

$$x_{\text{line}} = \left[i_{\text{line}D21} i_{\text{line}Q21}\right]. \tag{26}$$

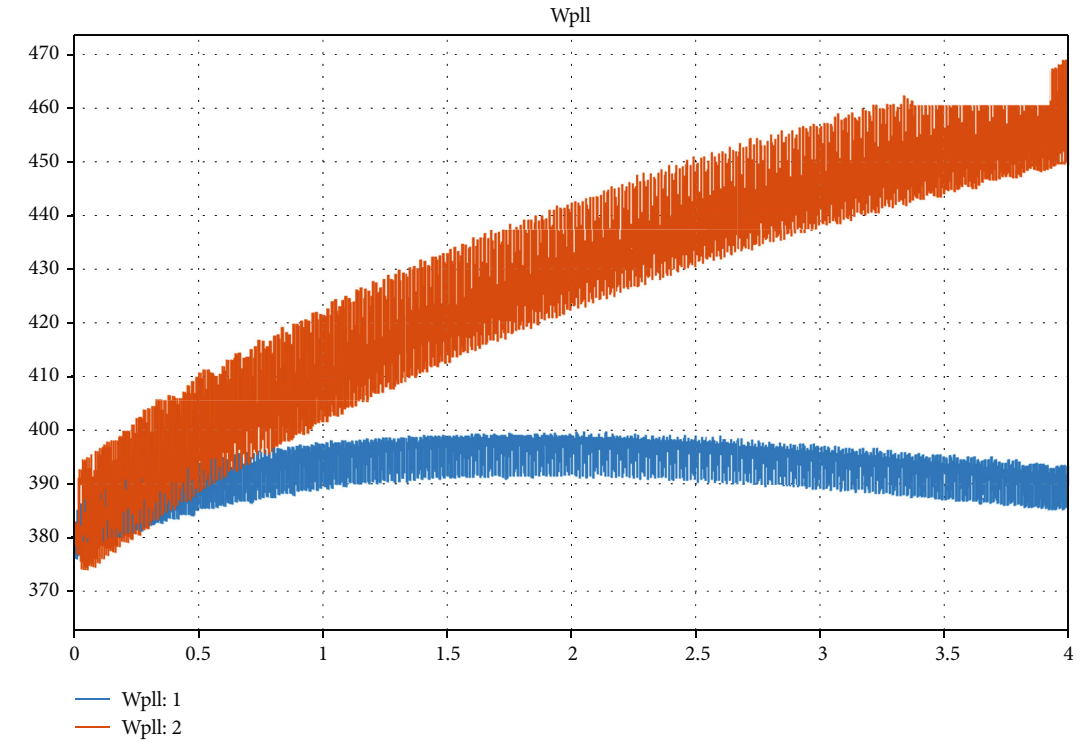

Figure 17: Angular rad/sec during unstable region.

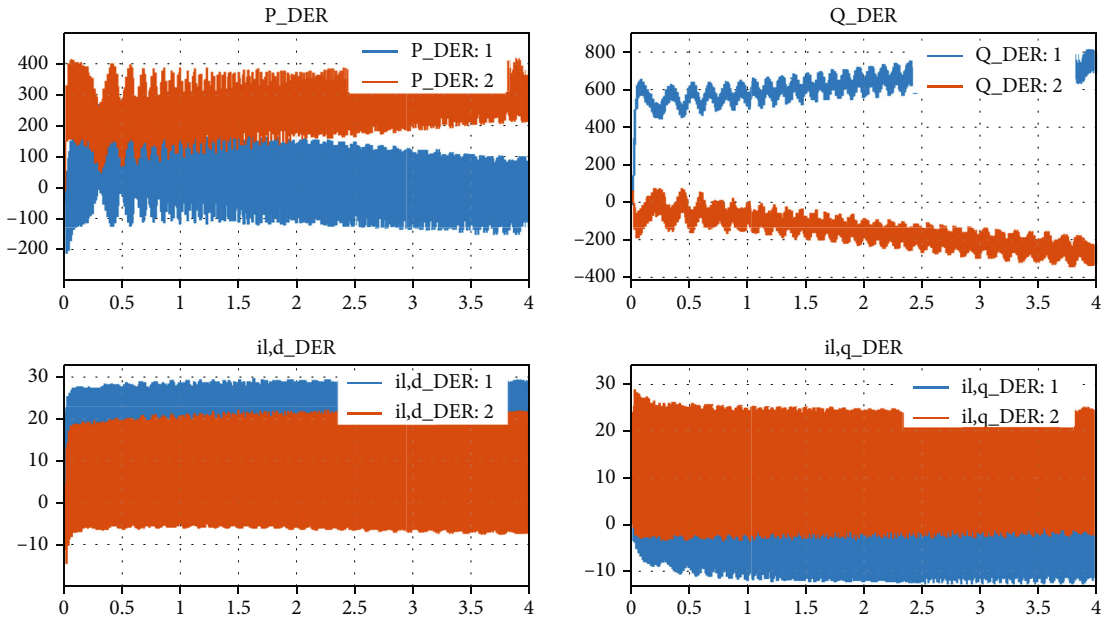

Figure 18: Real and reactive powers are unstable region.

By combining the vectors, one master vector is obtained as shown in

$$x = (x_{inv1} x_{inv2} x_{load} x_{line}]. \quad (27)$$

An operating point of the variables defined in Equation (27) is observed in the average model developed for linearization. These linearized values thus obtained are used for Eigen analysis. State space Equation (28) is developed using the master vector defined in Equation (27).

$$x = Ax + Bu, \quad (28)$$

where x is the state vector and u is the input. The input vector is given below. u = [vbD1 vbQ1 vbD2 vbQ2].

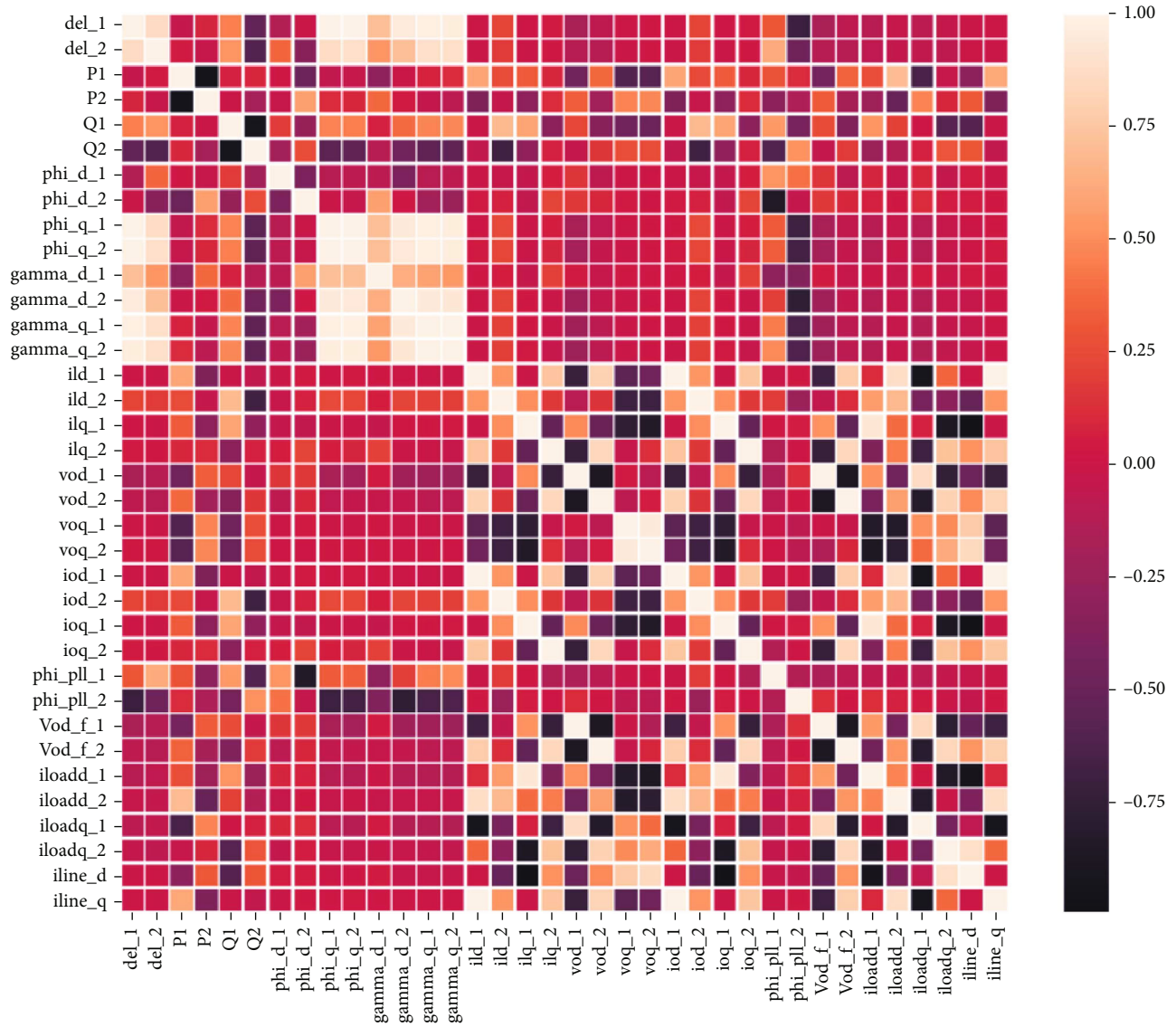

Figure 19: Heatmap of variables in (30) eigenvalues for state variables.

PCA analysis is applied to the variables to choose the total number of primary variables for stability analysis in the parallel inverter. Principal component analysis (PCA) is used as the dimensionality reduction procedure in machine learning applications. Larger number of variables is reduced to principal components (PC) which represent all the variables. Linear combination of all variables form the PCs. Stability analysis of the any system can be analyzed by means of Eigen analysis. Eigenvalues of the state space variables at steady state if positive it means that the system is unstable. While the eigenvalues if negative indicates that the system is stable. PCs are the eigenvalues of the state space variables. From the PCs the variables that affect the PCs can be found. Thus, finding the state space variables that affect the eigenvalues that determine the stability and instability of the system. The correlation diagram of all the 36 variables are as given in Figure 19.Waveform of the variables in Equation (27) are extracted. The extracted variables are plotted on a heat map in Figure 19 using Python to analyze PCA. The eigenvalues of the unstable operation are given in Table 2. Thus, for the stability analysis of the parallel inverters, top three variables can be accepted as the principal components.

Applying PCA to the number of variables in Equation (27) obtained during both stable and unstable regions, showed the three variables to be affecting the stability of the parallel inverters.

First step in PCA is standardizing the state space variables to a range of values. This is because PCA is sensitive to higher range of values which will lead to more affiliation to values with higher range. Space variables are normalized to be able to apply the PCA on the data. Matrix is generated to find the relation between the state space variables after standardization. Then vectors and values are computed from the matrix to obtain the principal components of the data. These PCs are uncorrelated and thus defining unique information about the data. For 36 state variables, 36 PCs will be available. But the first component will inherit maximum

Table 2: State variable eigenvalues at steady state.

Parameter	Eigenvalue
δ_1	$[-6.28087237e+01+0.j]$
δ_2	$[-3.38236020e+00+0.j]$
P_1	$[-2.07011345e-01+0.j]$
P_2	$[-9.6778641e-02+0.j]$
Q_1	$[-2.0002787e-02+0.j]$
Q_2	$[-3.78336738e-03+0.j]$
$\varphi\cdot_{d1}$	$[-1.9386353e-03+0.j]$
$\varphi\cdot_{d2}$	$[-8.78333632e-04+0.j]$
$\varphi\cdot_{q1}$	$[-3.948444725e-04+0.j]$
$\varphi\cdot_{q2}$	$[-2.0927252e-04+0.j]$
γ_{d1}	$[-9.636353563e-05+0.j]$
γ_{d2}	$[-6.093736637e-05+0.j]$
γ_{q1}	$[-4.73833663e-05+0.j]$
γ_{q2}	$[-3.383839829e-05+0.j]$
i_{ld1}	$[-2.838383333e-05+0.j]$
i_{ld2}	$[-1.33229282e-05+0.j]$
i_{lq1}	$[-6.82792911e-06+0.j]$
i_{lq2}	$[-9.6373627e-07+0.j]$
v_{od1}	$[-5.02920245e-07+0.j]$
v_{od2}	$[-4.95743920e-07+0.j]$
v_{oq1}	$[-1.23938022e-07+0.j]$
v_{oq2}	$[-1.0563929e-07+0.j]$
i_{od1}	$[-6.09729201e-08+0.j]$
i_{od2}	$[-3.04746379e-08+0.j]$
i_{oq1}	$[-1.0272611e-08+0.j]$
i_{oq2}	$[-5.08372729e-09+0.j]$

Table 3: State variables eigenvalues at an unstable state.

Parameter	Eigenvalues
δ_1	$[3.47599901e+01+0.j]$
δ_2	$[9.52223038e-01+0.j]$
P_1	$[1.78572064e-01+0.j]$
P_2	$[8.28196679e-02+0.j]$
Q_1	$[2.06535450e-02+0.j]$
Q_2	$[3.76254413e-03+0.j]$
$\varphi\cdot_{d1}$	$[9.30223166e-04+0.j]$
$\varphi\cdot_{d2}$	$[3.23647650e-04+0.j]$
$\varphi\cdot_{q1}$	$[2.74738000e-04+0.j]$
$\varphi\cdot_{q2}$	$[2.04843474e-04+0.j]$
γ_{d1}	$[7.96401036e-05+0.j]$
γ_{d2}	$[5.58565136e-05+0.j]$
γ_{q1}	$[4.43907914e-05+0.j]$
γ_{q2}	$[2.70049207e-05+0.j]$
i_{ld1}	$[1.98019468e-05+0.j]$
i_{ld2}	$[1.00697856e-05+0.j]$
i_{lq1}	$[6.62528703e-06+0.j]$
i_{lq2}	$[9.68277124e-07+0.j]$
v_{od1}	$[5.18866118e-07+0.j]$
v_{od2}	$[2.58497381e-07+0.j]$
v_{oq1}	$[1.81588836e-07+0.j]$
v_{oq2}	$[1.27296585e-07+0.j]$
i_{od1}	$[6.33469747e-08+0.j]$
i_{od2}	$[2.38383770e-08+0.j]$
i_{oq1}	$[8.57436145e-09+0.j]$
i_{oq2}	$[5.42819444e-09+0.j]$
$v_{od1,f}$	$[.72146918e-09+0.j]$
$v_{od2,f}$	$[.90209533e-09+0.j]$
i_{loadD1}	$[.00005811e-10+0.j]$
i_{loadD2}	$[.44779676e-10+0.j]$
i_{loadQ1}	$[.61968142e-10+0.j]$
i_{loadQ2}	$[.58108118e-10+0.j]$
$i_{lineD21}$	$[.70795635e-11+0.j]$
$i_{lineQ21}$	$[.61576758e-14+0.j]$

information about all the 36 variables to the maximum. And the information about the input variables in the PCs are found to be diminishing from second component. Percentage of variance of the state space variable is reflected in the PCs.

The first PC would exhibit the higher values of variance of the state space variables and it diminishes for the PCs further; the other PC values are negligible in percentage variance as they can be removed from the table.

4. Discussion

To choose the state space variables of importance principal components are scrutinized. The PC for 36 variables will be a 36×36 matrix. How each of the 36 state space variables affects the 36 PCs is defined. Since top three eigenvalues are contributing to most of the variance, only these three PCs are selected for further analysis.

Variables $\delta_{1,}\delta_{2,}$ and P_1 have higher eigenvalues as compared to other variables in Table 2. This exhibits that these variables can act as the principal components in obtaining the stability analysis of the parallel inverter topology in islanded mode. Thus, feature reduction in the implementation of stability analysis is evident from the PCA implementation. Although the PCA is affected by the variables, the stability will be affected by the variables that affects the PCs. Variables that affect the PCs can be obtained by plotting the coefficients of the variables that calculates the PCs. From Table 2, it can be observed that the principal

Table 4: State space variable and PC coefficients.

Parameter	PC coefficients
δ_1	0.06530153
δ_2	0.04732331
P_1	0.15161765
P_2	-0.08395888
Q_1	-0.03838542
Q_2	-0.02207935
$\varphi \cdot_{d1}$	-0.04568406
$\varphi \cdot_{d2}$	-0.00449388
$\varphi \cdot_{q1}$	0.06953892
$\varphi \cdot_{q2}$	0.07450347
γ_{d1}	0.01676722
γ_{d2}	0.06794937
γ_{q1}	0.06727851
γ_{q2}	0.06731414
i_{ld1}	0.27944524
i_{ld2}	0.11183713
i_{lq1}	-0.10433537
i_{lq2}	0.2636996
v_{od1}	-0.28665887
v_{od2}	0.28775177
v_{oq1}	-0.07699026
v_{oq2}	-0.0361415
i_{od1}	0.27949993
i_{od2}	0.11100814
i_{oq1}	-0.10424233
i_{oq2}	0.2634316
$v_{od1,f}$	.28355328
$v_{od2,f}$	28515001
i_{loadD1}	.09540814
i_{loadD2}	21144811
i_{loadQ1}	26672235
i_{loadQ2}	20395906
$i_{lineD21}$	10466113
$i_{lineQ21}$	28019509

components observed from the steady state variable are the linear combinations of the different variables thus obtained from the PCA. Correlation among the variables in the stability analysis needs to be removed by applying PCA. Correlated variables do not give more idea about the stability. Thus, finding the important variables that can highlight the stability of the system is necessary for feature reduction. PCs obtained from PCA analysis represent the uncorrelation between variables utilized in the stability analysis. Primary

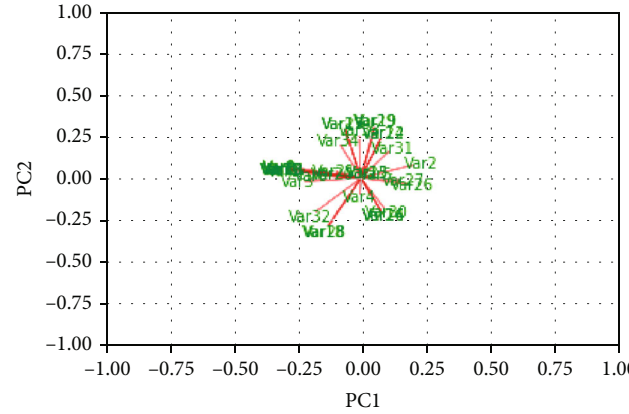

Figure 20: State variable PC1 and PC2 coefficient.

Table 5: Selected state space variables with high PC coefficients.

State space variable	Eigenvalues
i_{ld1}	$[5.15132354e+00+0.j]$
i_{lq2}	$[2.43332788e+00+0.j]$
v_{od2}	$[3.94566725e-01+0.j]$
i_{od1}	$[2.02298986e-02+0.j]$
i_{oq2}	$[5.07587063e-04+0.j]$
i_{loadD2}	$[2.89596201e-05+0.j]$
i_{loadQ1}	$[.55388696e-06+0.j]$
$i_{lineQ21}$	$[.85207779e-06+0.j]$

PCs obtained are PC1 and PC2. From the PCs, the variables with higher contribution to the PCs can be observed using PCA analysis. These variables affect the stability of the system both in the steady state and the transient state of the implementation. Stability analysis of the parallel inverter uses 36 variables. Negative eigenvalues indicate the stability of the system. Eigenvalues are the PCs in PCA. Variables that affect the first PC will eventually affect the stability of the system. The first PC represents around 96% of all the 36 variables. Depiction of the contribution of state variables to the PC1 and PC2 values is shown in Figure 19. State variables with higher contribution to PC1 are observed. These variables which contribute higher values to the PC1 value are extracted from the PC1 coefficients and those variables are further used for eigenanalysis of the system. The stability or instability of the system is analyzed by using the stipulated number of the state space variables instead of using the total state space variables coefficients of different state space variables are as given in Table 3. It can be observed that the variables i_{ld1}, i_{lq2}, v_{od2}, i_{od1}, i_{oq2}, i_{loadQ1}, and $i_{lineQ21}$ have higher PC coefficients. The Eigen analysis with variables corresponding to higher PC coefficients will be enough for the stability analysis of the system. These higher PC coefficients clearly indicate that those variables claim higher variance. The variables corresponding to higher PC coefficients are used for Eigen analysis of the overall system. The

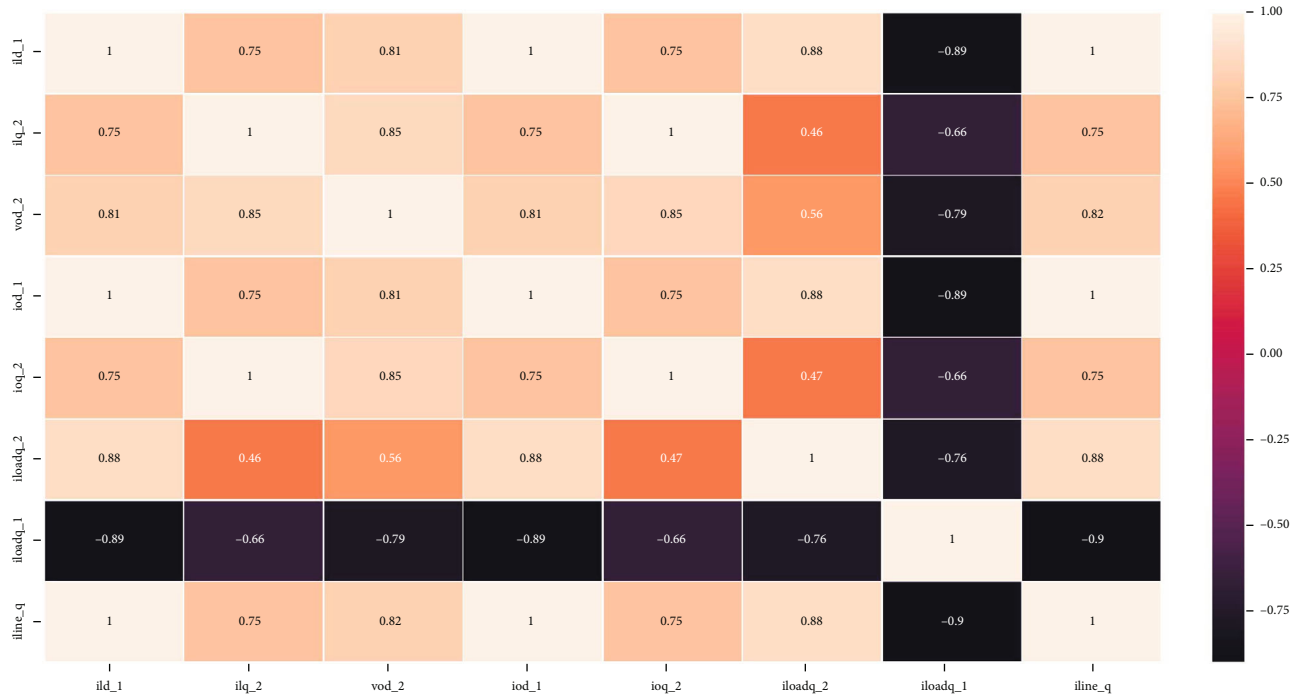

Figure 21: Heatmap of [4] state variables.

stability condition or the instability condition of both the reduced dimensional and without dimensionality reduction is found to be giving the same stability or instability condition. The PCA output from all 36 variables is obtained as PC1 and PC2 as given in Figure 19. As per PC1 and PC2 values are the coefficient values of the variables at the steady state. Both PC1 and PC2 values coefficient values for each variable are plotted to know the importance of the variables in Eigen analysis. The coefficient values of each variable tell the importance of these variables on the eigenvalues obtained that indirectly indicate the stability or instability in the system. Among all the variables, those values that are having higher coefficient values are chosen to determine the variables or state space variables that affect the stability of the system. The unstable region of the output is considered, and the eigenvalues are as given in Table 3.

The PCs are obtained by the linear combinations of the state space variables and the PC coefficients. PC coefficients represent the importance of those variables in the principal components. The PC coefficients for all the state variables are as given in Table 4.

Similarly, the eigenvalues of the 8 variables are positive to indicate that the system is unstable as the output obtained from the 36 variables. Table 4 shows the variables and their corresponding eigenvalues from the linearized average model of the parallel inverters.

The correlation graphs obtained from the heatmap of the implementation show that the correlation values between these 8 variables chosen from the PCA implementation is having good correlation values between them. And the stability analysis of the system using these 8 variables also depict that the system is in an unstable region. Eigenvalues of all the 8 variables are positive as is the same when applied with 36 variables. The correlation values between those 8 variables with higher PC coefficients are given in Figure 20. The correlation obtained between the eight state variables is shown in Figure 20.

These eight variables are selected using PCA from the 36 variables are clearly having moderate values unlike the 36 variables which had extreme values. Stability analysis of both the actual and feature-reduced analysis is found to be giving the same results. The primary PCs of both PC1 and PC2 are as shown in Figure 20. As per Table 5, the important variables that contribute to these primary PCs are taken, and the correlation diagram of these state variables are as shown in Figure 21.

5. Conclusion

Dimensionality reduction in the stability analysis of parallel inverters is implemented. Results obtained from PCA analysis indicated that the parallel inverters stability analysis does not require many variables as discussed in previous publications. The dimensionality reduction applied to the variables from the linearized average model indicated validation of dimensionality reduction. An average model developed using MATLAB and PCA is carried out using Python which clearly indicates the validation of the dimensionality reduction in the stability analysis. The reduced number of variables is validated for both the stable and unstable range of the parallel inverter droop controller. Both cases validated dimensionality reduction in the stability analysis of parallel inverters.

Feature reduction for stability analysis in the future can lead to a reduction in the need for more variables needed for stability analysis of the complex system. Memory

allocation for the stability analysis will get reduced due to a lesser number of variables. In future work, the dynamics of photovoltaic characteristics can be introduced in the implementation to obtain the in-situ dynamics of the microgrids. This can be extended to other renewable sources which is having voltage at the DC link to be varying. Other feature extraction algorithms like linear discriminant analysis (LDA) can be implemented instead of PCA to get further insights into the variables that affect the stability analysis of the islanded mode converters. Other renewable energy sources like wind turbines and tidal can be introduced by introducing the dynamics of the renewable sources. Since the DC link voltage of the parallel inverters used in the implementation is constant, it is meant for only the constant DC supply at the DC link. Introducing the dynamics of renewable energy resources gives a better idea about the stability of the system.

Abbreviation

P: Real power
p: Real power (instantaneous)
Q: Reactive power
q: Reactive power (instantaneous)
ω_c: Corner frequency
v_{od}: Direct axis voltage (inverter)
v_{oq}: Quadrature axis voltage (inverter)
i_{od}: Direct axis current (inverter)
i_{oq}: Quadrature axis current (inverter)
m, n: Droop real power-angular radian/sec and reactive power-voltage slope, respectively
c, PLL: Reference corner frequency
$k_{p,\ \mathrm{PLL}}$: Proportional parameters for PLL generation
i_{ld}: Direct axis current (line)
i_{lq}: Quadrature axis current (line)
L_f: Inductor (filter)
L_c: Inductance
r_f; r_c: Parasitic resistance
R_{load}: Load resistance
L_{load}: Load inductance
δ_1: Phase angle reference for master inverter
δ_2: Phase angle slave inverter.

Data Availability

The data that support the findings of this study are available on request from the corresponding author.

Conflicts of Interest

The authors have no conflicts of interest to declare.

References

[1] A. Rodríguez-Cabero and M. Prodanovic, "Stability analysis for weak grids with power electronics interfaces. IECON Proceedings," in *IECON 2016 - 42nd Annual Conference of the IEEE Industrial Electronics Society*, pp. 2402–2407, Florence, Italy, 2016.

[2] L. Araújo, M. G. Villalva, and T. G. Siqueira, "Autonomous microgrid with en- ergy stor- age system," in *IEEE 26th International Symposium on Industrial Electronics (ISIE*, pp. 57–62, Edinburgh, UK, 2017.

[3] J. Lai, X. Lu, X. Li, and R. Tang, "Distributed multiagent-oriented average control for voltage restoration and reactive power sharing of autonomous microgrids," *IEEE Access.*, vol. 6, pp. 25551–25561, 2018.

[4] S. Leonori, M. Paschero, F. M. F. Mascioli, and A. Rizzi, "Optimization strategies for microgrid energy management systems by genetic algorithms," *Applied Soft Computing.*, vol. 86, pp. 105903–105903, 2020.

[5] M. Gheisarnejad and M. H. Khooban, "Secondary load frequency control for multi-microgrids: HiL real-time simulation," *Soft Computing.*, vol. 23, no. 14, pp. 5785–5798, 2019, Available from:.

[6] A. Firdaus and S. Mishra, "A double derivative-based droop controller for improved power sharing in inverter based autonomous microgrid," in *2018 IEEMA Engineer Infinite Conference (eTechNxT)*, pp. 1–6, New Delhi, India, 2018.

[7] F. Zandi, B. Fani, I. Sadeghkhani, and A. Orakzadeh, "Adaptive complex virtual impedance control scheme for accurate reactive power sharing of inverter interfaced autonomous microgrids," *IET Generation, Transmission & Distribution.*, vol. 12, no. 22, pp. 6021–6032, 2018, Available from:.

[8] M. Rasheduzzaman, J. A. Mueller, and J. W. Kimball, "An accurate small-signal model of inverter- dominated islanded microgrids using dq reference frame," *Electronics*, vol. 2, no. 4, pp. 1070–1080, 2014, Available from:.

[9] K. Veerashekar, S. Eichner, and M. Luther, "Modelling and transient stability analysis of interconnected autonomous hybrid microgrids," in *2019 IEEE Milan PowerTech*, pp. 1–6, Milan, Italy, 2019.

[10] B. Dag and M. Aydemir, "A simplified stability analysis method for LV inverter-based microgrids," *Journal of Modern Power Systems and Clean Energy.*, vol. 7, no. 3, pp. 612–620, 2019.

[11] Y. Wang, X. Wang, F. Blaabjerg, and Z. Chen, "Harmonic instability assessment using atate-space modeling and participation analysis in inverter-fed power systems," *IEEE Transactions on Industrial Electronics*, vol. 64, no. 1, pp. 806–816, 2017.

[12] H. Alenius, M. Berg, R. Luhtala, T. Roinila, and T. Messo, "Impedance- based stability analysis of multi-parallel inverters applying total source admittance," in *2019 20th Workshop on Control and Modeling for Power Electronics (COMPEL)*, pp. 1–8, Toronto, ON, Canada, 2019.

[13] X. Zhang, H. Chung, L. L. Cao, J. Chow, and W. Wu, "Impedance- based stability criterion for multiple offshore inverters connected in parallel with long cables," in *2017 IEEE Energy Conversion Congress and Exposition (ECCE)*, vol. 2017, pp. 3383–3389, Cincinnati, OH, USA, 2017.

[14] M. Amin and M. Molinas, "Small-signal stability assessment of power electronics based power systems: a discussion of impedance- and eigenvalue-based methods," *IEEE Transactions on Industry Applications.*, vol. 53, no. 5, pp. 5014–5030, 2017, Available from:.